


## Procrustean entanglement concentration in quantum-classical networking

Hsuan-Hao Lu<sup>1,\*</sup>, Muneer Alshowkan<sup>1</sup>, Jude Alnas<sup>2</sup>, Joseph M. Lukens<sup>1,3</sup> and Nicholas A. Peters<sup>1</sup>

<sup>1</sup>*Quantum Information Science Section, Computational Sciences and Engineering Division, Oak Ridge National Laboratory, Oak Ridge, Tennessee 37831, USA*

<sup>2</sup>*Department of Electrical and Computer Engineering, Duke University, Durham, North Carolina 27708, USA*

<sup>3</sup>*Research Technology Office and Quantum Collaborative, Arizona State University, Tempe, Arizona 85287, USA*

 (Received 15 December 2023; revised 2 March 2024; accepted 21 March 2024; published 15 April 2024)

The success of a future quantum internet will rest in part on the ability of quantum and classical signals to coexist in the same optical fiber infrastructure, a challenging endeavor given the orders of magnitude differences in flux of single-photon-level quantum fields and bright classical traffic. We theoretically describe and experimentally implement Procrustean entanglement concentration for polarization-entangled states contaminated with classical light, showing significant mitigation of crosstalk noise in dense wavelength-division multiplexing. Our approach leverages a pair of polarization-dependent loss emulators to attenuate highly polarized crosstalk that results from imperfect isolation of conventional signals copropagating on shared fiber links. We demonstrate our technique both on the tabletop and over a deployed quantum local area network, finding a substantial improvement of two-qubit entangled state fidelity from approximately 75% to over 92%. This local filtering technique could be used as a preliminary step to reduce asymmetric errors, potentially improving the overall efficiency when combined with more complex error-mitigation techniques in future quantum repeater networks.

DOI: [10.1103/PhysRevApplied.21.044027](https://doi.org/10.1103/PhysRevApplied.21.044027)

### I. INTRODUCTION

Quantum-classical coexistence within fiber-optic resources will streamline the implementation of quantum networks, enabling efficient utilization of infrastructure and reducing deployment costs. One promising pathway relies on distinguishing classical and quantum channels by wavelength. Although originally pursued through coarse wavelength-division multiplexing (CWDM) [1–6], quantum-classical coexistence efforts are increasingly targeting dense wavelength-division multiplexing (DWDM) with channels of 200 GHz or less, for even greater spectral efficiency [7–14]. Given the stark contrast in brightness between classical and quantum signals, such ultratight spacings are highly susceptible to imperfect filter isolation and unwanted noise infiltrating the quantum output [7, 8, 12, 14]. At whatever level of crosstalk is present, the strong temporal correlations between entangled photons can be leveraged to some extent for filtering uncorrelated noise by reducing the coincidence detection window. Nevertheless, the timing jitter between two nodes ultimately determines how narrow this window can be before genuine coincidences are lost, a limitation becoming especially pronounced in geographically separated nodes where timing

jitters are constrained by the capabilities of the timing electronics [5, 15].

In this paper, we introduce a crosstalk mitigation method tailored to polarization-entangled photons tainted by highly polarized classical signals, a practical source of error from typically polarized conventional communications signals. For appropriate orientations, the noisy density matrix maps approximately to the class of maximally entangled mixed states (MEMS) [16–18], whose entanglement can be concentrated through local “Procrustean” filtering [18–21]. Additionally, our approach resembles the polarization-dependent loss (PDL) compensation possible for Bell states [22–24], whereby reductions in concurrence due to PDL on one photon can be completely compensated (in postselection) by applying PDL of an appropriately chosen orientation and magnitude to the other. This situation facilitates the filtering of noisy quantum states while retaining maximal entanglement in the Bell-state portion and suppressing nonentangled terms. After simulating a general model, we experimentally demonstrate the approach with programmable polarization-dependent loss emulators (PDLEs; OZ Optics) applied to entangled photons contaminated with crosstalk from copropagating lasers. In all cases examined—both on the optical table and over a deployed network—fidelity is found to increase in good agreement with theory. Overall, our method provides

\*Corresponding author. [luh2@ornl.gov](mailto:luh2@ornl.gov)

an additional error-mitigation layer for quantum-classical coexistence networks that can be applied, e.g., for dynamic removal of asymmetric noise.

## II. MOTIVATION

Figure 1 illustrates the proposed scheme. Consider an ideal Bell state  $|\Phi^+\rangle = 1/\sqrt{2}(|HH\rangle + |VV\rangle)$  as the input, where  $|H\rangle$  ( $|V\rangle$ ) denotes a horizontally (vertically) polarized state. Following generation, signal and idler photons are physically separated into two optical arms destined for Alice ( $A$ ) and Bob ( $B$ ), each combined with highly polarized classical traffic through a DWDM multiplexer (MUX). Upon reaching the receivers, photons are wavelength-demultiplexed using another DWDM demultiplexer (DEMUX). Due to imperfect spectral filtering and channel isolation, the quantum channel now includes a small portion of classical crosstalk noise. Alice and Bob send their respective signals through a PDLE module designed to controllably replicate PDL in optical links [25,26]. The PDLE module spatially separates the input into two orthogonal polarizations, applying user-defined attenuation to one of them, referred to as the PDL axis, while passing the other unaltered. The two polarizations are then recombined into a single fiber-optic spatial mode at the output.

To optimize the noise suppression possible with PDLEs, intuition suggests orienting the PDL axes orthogonally ( $H/V$ ) with respect to the initial reference frame to ensure equal attenuation of the terms of interest in  $|\Psi^+\rangle$ , while aligning the classical traffic to these axes for greatest suppression. In this scenario, a reasonable approximation of the initial noisy quantum state (before any PDL) is  $\rho \approx \gamma |\Phi^+\rangle \langle \Phi^+| + (1 - \gamma) |HV\rangle \langle HV|$ , where  $\gamma \in [0, 1]$  defines the relative weight of accidentals stemming from the noise photons in comparison to the genuine coincidences between the entangled pairs. For  $\gamma \in [2/3, 1]$  this state is precisely that of the MEMS I subclass [16–18],

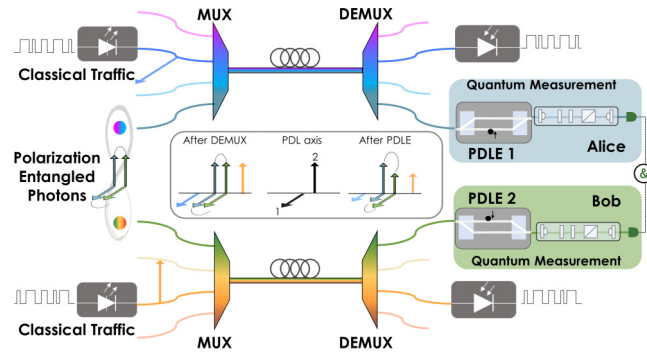


FIG. 1. Concept of Procrustean filtering for polarization-entangled photons. Crosstalk suppression can be achieved by aligning the PDLE axes and classical traffic polarizations accordingly.

which is a sufficient (though not necessary) criterion for our concentration method.

With the introduction of two PDLEs imparting variable transmissivities  $T_H, T_V \in [0, 1]$  along their respective PDL axes, the output density matrix becomes  $\rho \propto \gamma (\sqrt{T_H} |HH\rangle + \sqrt{T_V} |VV\rangle) (\sqrt{T_H} \langle HH| + \sqrt{T_V} \langle VV|) + (1 - \gamma) T_H T_V |HV\rangle \langle HV|$ . Notably, the unwanted term  $|HV\rangle \langle HV|$  decreases more rapidly than the rest of the matrix entries as  $T_H$  and  $T_V$  decrease. In particular, the fidelity with respect to the maximally entangled ideal ( $\mathcal{F} = \langle \Phi^+ | \rho | \Phi^+ \rangle$ ) approaches unity as  $T_H = T_V \rightarrow 0$ , implying an arbitrary increase (at the expense of flux). Now, this model is only approximate in that it neglects other noise terms, such as coincidences *between* crosstalk and input photons, but it summarizes the basic concept. In the following, we introduce the more complete model accounting for all accidental contributions in the system of interest.

## III. MODEL

Consider polarization-entangled photons generated in the state  $|\Phi^+\rangle$  at rate  $\mu$ . Subsequently, the idler (signal) photon is separated into optical arm  $A$  ( $B$ ) with pathway efficiency  $\eta_A$  ( $\eta_B$ ) encompassing all loss effects from generation through detection. The rate of photon detection from classical crosstalk is  $\nu_A$  ( $\nu_B$ ) in arm  $A$  ( $B$ ) when the polarization analyzer is aligned to  $H$  ( $V$ ) and  $T_H = 1$  ( $T_V = 1$ ). Additionally, we consider dark counts at detector  $A$  ( $B$ ) with rate  $d_A$  ( $d_B$ ). The coincidence window is set to  $\tau$ , with the assumption that this window is significantly longer than the two-photon temporal correlations.

Under these conditions, the complete received quantum state can be written as

$$\begin{aligned} \rho = \frac{1}{R} & \left\{ \frac{\mu \eta_A \eta_B}{2} (\sqrt{T_H} |HH\rangle + \sqrt{T_V} |VV\rangle) \right. \\ & \times (\sqrt{T_H} \langle HH| + \sqrt{T_V} \langle VV|) \\ & + \tau \left[ \frac{\mu \eta_A}{2} (T_H |H\rangle \langle H| + |V\rangle \langle V|) \right. \\ & + \nu_A T_H |H\rangle \langle H| + d_A I_2 \left. \right] \\ & \otimes \left[ \frac{\mu \eta_B}{2} (|H\rangle \langle H| + T_V |V\rangle \langle V|) \right. \\ & \left. + \nu_B T_V |V\rangle \langle V| + d_B I_2 \right] \left. \right\}, \end{aligned} \quad (1)$$

where  $I_2$  is the  $2 \times 2$  identity and  $R$  denotes the coincidence rate over all outcomes in a basis, such that  $\text{Tr} \rho = 1$ . The quantum state contains a correlated term from photons in the same pair (scaled by  $\mu \eta_A \eta_B$ ) and an uncorrelated term (scaled by  $\tau$ ), which can be derived following standard arguments for the rate of accidentals as the product of the rates on the individual detectors multiplied by  $\tau$

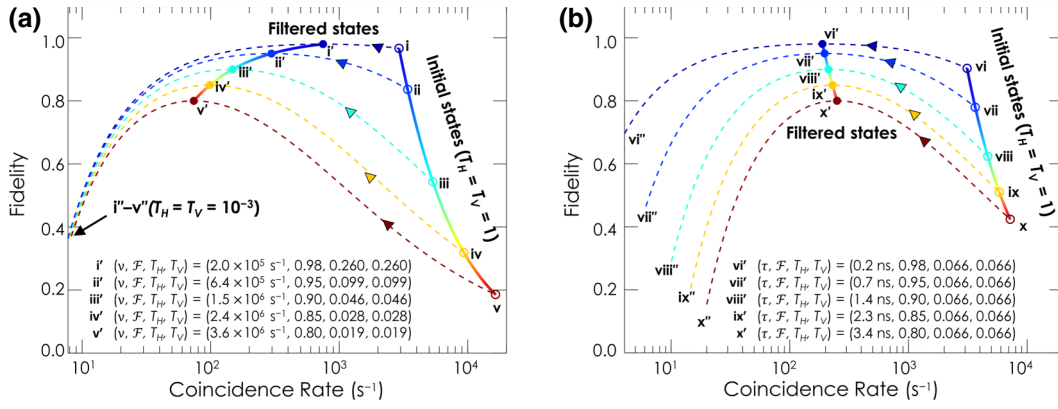


FIG. 2. Numerical simulation of Procrustean filtering with fixed parameters  $\{\mu, \eta_A, \eta_B, d_A, d_B\} = \{7 \times 10^6, 0.02, 0.02, 100, 100\}$ . (a) Variable noise rates  $\nu_A = \nu_B = \nu \in [2 \times 10^5, 3.6 \times 10^6]$  with a coincidence window  $\tau = 10^{-9}$ . (b) Variable coincidence window  $\tau \in [2 \times 10^{-10}, 3.4 \times 10^{-9}]$  with a noise rate of  $\nu_A = \nu_B = 10^6$ . Solid curves represent initial noisy states (right) and optimized filtered states (left). Dashed curves illustrate state evolution as  $T_H = T_V$  is scanned from 1 to  $10^{-3}$ .

[27,28]—valid in the limit of small detection probabilities. The noise term thereby consists of a product of the marginal states at each detector, in brackets  $[\cdot]$  in Eq. (1), each of which contains three contributions: (i) partially polarized light from the filtered entangled photons (scaled by  $\mu\eta_{A(B)}$ ), (ii) attenuated linearly polarized light from classical crosstalk ( $\nu_{A(B)}$ ), and (iii) white noise from detector dark counts ( $d_{A(B)}$ ).

Due to the physical effects reflected in (i) and (iii), Eq. (1) no longer matches a true MEMS I form, yet the classical crosstalk term (proportional to  $\nu_A\nu_B$ ) can still be selectively suppressed relative to the correlated term. If  $T_H = T_V = T$ , for example, the flux from the former drops quadratically ( $T^2$ ), while the latter only linearly ( $T$ ). Thus, whenever noise is dominated by classical crosstalk, the fidelity with respect to  $|\Psi\rangle$  can be increased by reducing  $T_H$  and  $T_V$ . However, as  $T$  decreases, at some point the multipair (i) and dark count effects (iii) will take over; for example, the extreme case of  $T_H = T_V = 0$  would completely suppress the crosstalk but lead to a separable state:  $\rho \propto (\mu\eta_A/2|V\rangle\langle V| + d_A I_2) \otimes (\mu\eta_B/2|H\rangle\langle H| + d_B I_2)$ . Consequently, for any state of the form in Eq. (1), there exists an optimal pair of PDLE filters  $(T_H, T_V)$  to maximize  $\mathcal{F}$ .

In Fig. 2(a), we model these tradeoffs in a scenario with a pair rate of  $\mu = 6 \times 10^6 \text{ s}^{-1}$ , pathway efficiencies  $\eta_A = \eta_B = 0.02$ , dark count rates of  $d_A = d_B = 100 \text{ s}^{-1}$ , and a coincidence window of  $\tau = 1 \text{ ns}$ . We introduce variable noise in both arms, with  $\nu_A = \nu_B = \nu \in [2, 36] \times 10^5 \text{ s}^{-1}$ . The five points (Roman numerals i–v) in Fig. 2(a) correspond to distinct crosstalk levels  $\nu$  with no filtering applied ( $T_H = T_V = 1$ ) and represent initial noisy quantum states. For each of these cases, we numerically find the  $(T_H, T_V)$  pair that maximizes  $\mathcal{F}$ , which are shown as primed values (i'–v') and reach  $\mathcal{F} \in \{0.98, 0.95, 0.90, 0.85, 0.80\}$ . Our results consistently indicate the optimal filtering occurs

when  $T_H = T_V$ , aligning with the case for ideal MEMS I states. We also illustrate the state evolution concerning PDLE filtering by mapping the fidelity-rate trajectories for  $T_H = T_V = T \in [0.001, 1]$ , as represented by the dashed curves. The maximum attainable fidelity, along with the optimal filtering levels, depends on the noisiness of the initial states. Beyond this threshold,  $\mathcal{F}$  decreases as the multipair effect (the unfiltered  $|VH\rangle\langle VH|$  term) increasingly dominates.

Likewise, the influence of crosstalk varies as the coincidence window  $\tau$  changes. In Fig. 2(b), we consider a scenario where photon flux and background levels are fixed at  $(\mu, \eta_A, \eta_B, \nu_A, \nu_B, d_A, d_B) = (7 \times 10^6 \text{ s}^{-1}, 0.02, 0.02, 10^6 \text{ s}^{-1}, 10^6 \text{ s}^{-1}, 100 \text{ s}^{-1}, 100 \text{ s}^{-1})$ , while  $\tau$  varies in  $[0.2, 3.4] \text{ ns}$ . We again assume the biphoton temporal correlation is significantly shorter than  $\tau$ , so increasing  $\tau$  only includes more accidentals from two random clicks between the detectors. As expected, the optimal fidelity is contingent upon the noisiness of the original state. Nevertheless, the optimal filtering configuration  $(T_H, T_V)$  remains consistent across all cases.

#### IV. TABLETOP EXPERIMENTS

Figure 3 illustrates the experimental setup. Broadband, polarization-entangled photons are separated by a C- and L-band demultiplexer, with signal and idler photons covering the optical C band (1530–1565 nm) and L band (1565–1625 nm), respectively (detailed design outlined in Ref. [29,30]). In each fiber arm, we program a wavelength-selective switch (WSS; Finisar) operated in reverse to accept a 25-GHz-wide energy-matched channel pair: 193.9 THz in the C band and 189.1 THz in the L band. For all scenarios tested, we measure coincidences (5 s per point in the tabletop experiments, 10 s in the deployed tests) in an overcomplete set of 36 polarization projections using a pair of

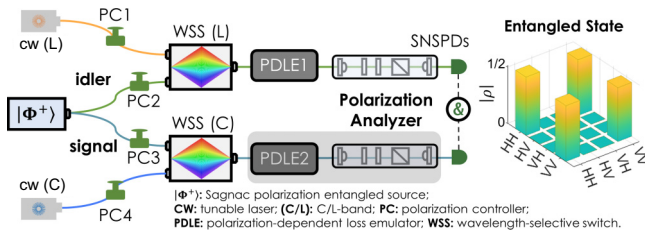


FIG. 3. Experimental setup and Bayesian mean density matrix of the initial entangled resource. The gray shaded box (PDLE2 and the polarization analyzer in the signal arm) was relocated to another building in the deployed network test. See text for details.

motor-controlled polarization analyzers [29,30], comprising a quarter-wave plate, half-wave plate, and polarizing beamsplitter. Bayesian quantum state tomography (QST) [31,32], following the refinements in likelihood and prior outlined in Ref. [33], is then applied to recover density matrix samples. Without any crosstalk and a coincidence window  $\tau = 1.4$  s, we find the mean density matrix in Fig. 3, with fidelity  $\mathcal{F} = 0.988(1)$ .

After establishing this initial entangled resource, we introduce classical crosstalk using a pair of tunable, linearly polarized cw lasers, operating at frequencies of 189.125 THz [cw (L) in Fig. 3] and 193.925 THz [cw (C) in Fig. 3], respectively, i.e., one frequency slot away from their respective quantum channel on the 25 GHz ITU grid (ITU-T Rec. G.694.1). To emulate the narrow-band filtering necessary for future coexistence networks, both lasers are heavily attenuated. At each receiver, we record  $\nu \approx 4.5 \times 10^5 \text{ s}^{-1}$ —approximately 10 times more than the detection rate due to photons from entangled pairs—chosen to introduce an aggressive amount of accidentals while avoiding saturation of the superconducting nanowire single-photon detectors (SNSPDs).

To demonstrate the method for maximum improvement relies on two levels of coordination in polarization: first, the PDL axis at each receiver must be aligned to the polarization of the classical crosstalk; second, the polarization

correlations for the crosstalk contributions must be orthogonal to the correlations in the Bell state of interest. Once the former is achieved, the latter can in principle be realized through local rotation of only one photon from the maximally entangled pair (prior to multiplexing) [34,35]. Nonetheless, for ease of implementation here, we manually tune the polarization of all four inputs relative to fixed PDL axes [via polarization controllers (PCs) 1–4 in Fig. 3]; this allows us to produce a state in the form of Eq. (1), up to a relative phase between  $|HH\rangle$  and  $|VV\rangle$  in the Bell-state term. Any residual phase is automatically compensated by the local rotations we apply to the inferred density matrices in postprocessing, chosen to maximize fidelity with respect to  $|\Phi^+\rangle$  [29]. The resulting noisy state measured with  $\tau = 1.4$  ns is depicted in Fig. 4(a) (labeled i) and resembles a MEMS I state [16–18].

For the above and all experimental results below, we estimate the output density matrix  $\rho$  and flux  $R$  with no reference to Eq. (1); the states are inferred from a completely uniform Bures prior without assuming any particular noise model [33]. However, to extract critical parameters of interest for validating our model, for this particular case only ( $T_H = T_V = 1$  and  $\tau = 1.4$  ns) we perform an additional inference step in which we temporarily assume Eq. (1) to infer the parameters  $(\mu, \eta_A, \eta_B, \nu_A, \nu_B)$ , which are difficult to measure independently. For this purpose, we develop a customized Bayesian model patterned after Ref. [36] that considers both single-detector events and coincidences, takes as input the independently measured dark count rates at  $d_A = d_B = 100 \text{ s}^{-1}$ , and places normal priors on the four unknowns of interest  $(\mu, \eta_A, \eta_B, \nu_A, \nu_B)$ , with means given by our initial estimates from the count data, and standard deviations equal to 10% of these values. Under this “open box” model [36,37], we obtain  $(\mu, \eta_A, \eta_B, \nu_A, \nu_B) = [5.889(3) \times 10^6 \text{ s}^{-1}, 2.113(1) \times 10^{-2}, 1.375(2) \times 10^{-2}, 4.152(1) \times 10^5 \text{ s}^{-1}, 4.653(2) \times 10^5 \text{ s}^{-1}]$ , which, in conjunction with Eq. (1), serve as the basis for subsequent theory curves. To effectively concentrate this noisy state, we utilize two PDLE modules (with approximately 1-dB residual loss) to

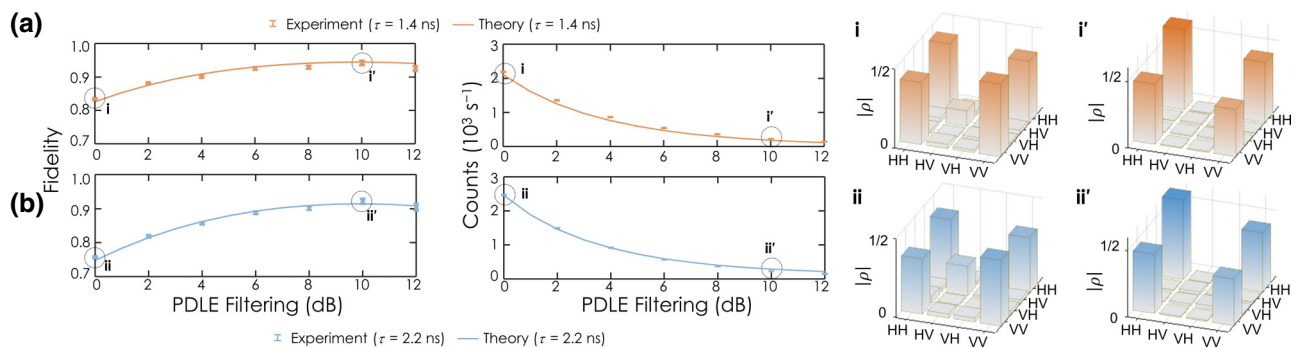


FIG. 4. Bayesian state fidelities and collected coincidences versus PDLE local filtering. Measured density matrices at (i,ii) 0 dB ( $T_H = T_V = 1$ ) and (i',ii') 10 dB ( $T_H = T_V = 0.1$ ) of PDL. Coincidence window  $\tau$ : (a) 1.4 ns, (b) 2.2 ns.

implement Procrustean filtering on the multiplexed channel. To optimize state fidelities, we set both PDLEs to the same filtering level throughout the experiment (i.e.,  $T_H = T_V = T$ ), which aligns with the observations made in the previous sections.

Figure 4(a) depicts the state evolution as the PDLE filtering level is increased from 0 dB ( $T = 1$ ) to 12 dB ( $T = 0.063$ ) in 2-dB steps. The fidelity advances steadily from  $\mathcal{F}_{0 \text{ dB}} = 83.4(3)\%$  to  $\mathcal{F}_{10 \text{ dB}} = 94.2(7)\%$  [Fig. 4(a)], at the expense of reduced flux [Fig. 4(b)]. Incidentally, the linear entropy decreases from 0.384(5) to 0.10(2), while the tangle increases from 0.57(1) to 0.81(3), confirming true entanglement “concentration” as defined as increases in both entanglement and purity [18,38]. We halt the investigation at 12 dB as we have observed that, for our particular system parameters, the fidelity reaches a plateau within the range of 10–12 dB, as predicted by the accompanying theory. Beyond this point, the fidelity begins to decline due to the accidentals from multipair emission, as discussed previously.

To examine noisier state, we widen the coincidence window to  $\tau = 2.2$  ns, resulting in a roughly 60% increase in accidentals [cf. Eq. (1)]. The results, depicted in Fig. 4(b), show Procrustean fidelity improvements from  $\mathcal{F}_{0 \text{ dB}} = 75.8(3)\%$  to  $\mathcal{F}_{10 \text{ dB}} = 92.2(8)\%$ . Additionally, the overall trend and optimal filtering level closely match those observed in the case of Fig. 4(a) when  $\tau = 1.4$  ns, which aligns with our findings in Fig. 2(b).

## V. DEPLOYED NETWORK TESTS

We next apply our method in a deployed quantum local area network on the Oak Ridge National Laboratory campus [15,39]. The source and components in the idler arm remain in the original lab (Alice in Refs. [15,39]), while PDLE2 and the polarization analyzer in the signal arm are relocated to another building (Bob in Ref. [15,39]). A deployed fiber link, approximately 250 m long with a round-trip loss of approximately 5 dB, connects the two buildings. After polarization projections, signal photons are routed back to Alice for photon detection. We transmit Bob’s projected photons back to Alice—rather than detect them at Bob—due to the availability of SNSPDs; Bob’s avalanche photodiodes considered in previous experiments [15,39] approach saturation at the level of crosstalk noise of interest here.

As a further modification from the tabletop experiment, we tune the classical crosstalk lasers from their original positions at 189.125 THz and 193.925 THz (25 GHz away from their respective quantum channels) to the center of their respective quantum channels at 189.1 THz and 193.1 THz. Now, the Procrustean filtering approach described here places no requirements on the specific wavelength of the crosstalk, as long as it is polarized and copropagating with the demultiplexed quantum output.

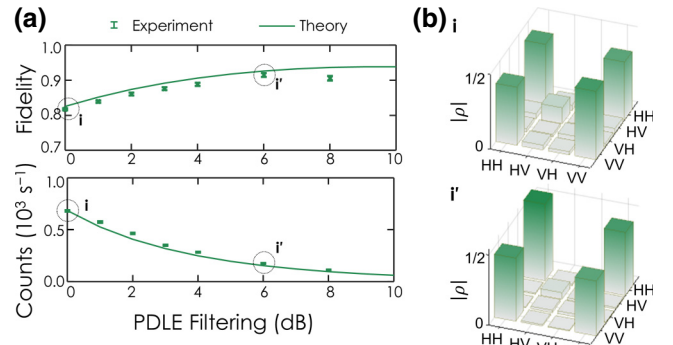


FIG. 5. (a) Bayesian-estimated fidelities and flux versus PDLE local filtering in a deployed network setting. (b) Measured density matrices at (i) 0 dB and (i') 6 dB PDL.

Thus, whether stemming from imperfect isolation of a nearby frequency (emulated in Fig. 4) or from background light that truly spectrally overlaps with the quantum signal (emulated in Fig. 5), all that matters is its overall polarized contribution to the total rate of received photons, as quantified by  $\nu_A$  and  $\nu_B$  in Eq. (1). Consequently, by shifting the laser frequencies for the deployed experiment, we supplement the *out-of-band* crosstalk tests in Fig. 4 with *in-band* crosstalk as well, finding no qualitative differences between the two (as confirmed below).

Figure 5 summarizes the experimental results obtained from our deployed network. In this case, Procrustean filtering improves the entangled state resource from  $\mathcal{F}_{0 \text{ dB}} = 81.7(3)\%$  to  $\mathcal{F}_{6 \text{ dB}} = 91.5(5)\%$ , which so happens to transition the distributed entangled state from a regime where quantum key distribution (QKD) is impossible to one where it may be performed. The BB84 QKD protocol using one-way communication possesses an 11% quantum bit error rate (QBER) threshold [40–42]; the QBERs associated with the initial state are 13.8(4)% and 12.2(4)% for the rectilinear and diagonal bases, respectively, but they decrease to 6.6(6)% and 3.8(6)% for the 6-dB filtered state.

## VI. DISCUSSION

In this study, we have employed fidelity as the key metric to assess the effectiveness of Procrustean filtering. However, our model can be adapted to optimize other metrics that are computable from the density matrix as well [43–46]. Expanding our analysis, we could employ constrained nonlinear optimization to explore more complex scenarios, such as maximizing total coincidence rates while constraining fidelity above a predefined application-specific threshold [47,48]. Such an approach can be particularly valuable in photon-starved applications where optimizing both throughput and quality of entanglement are essential.

Procrustean filtering should not be construed as an alternative to CWDM and DWDM or time-division multiplexing but rather an additional layer that can supplement such strategies to further mitigate the impact of classical crosstalk in shared optical fiber. By coordinating the relative orientations of entangled photons and coexisting classic traffic—possible through control of the polarization of either the quantum or classical input (full control of both signals is not required)—the two-photon correlations possessed by the quantum and classical portions are distinct and can be selectively filtered when multiplexed in shared fiber. Accordingly, while our procedure does presuppose polarization coordination between coexisting quantum and classical signals and so does not address cases of highly unpolarized noise (Raman scattering being a common example [6,7,12]), the benefits it engenders are still quite general, applying to any operating condition in which the dominant crosstalk is polarized. Such cases can lead to asymmetric errors in the quantum state, making this local filtering technique a potentially valuable preliminary step, in tandem with other error-reduction techniques, for improving entanglement distribution efficiency in future quantum repeater networks.

### ACKNOWLEDGMENTS

We thank Y. Zhang for helpful discussions regarding QBER thresholds. This work was performed in part at Oak Ridge National Laboratory, operated by UT-Battelle for the U.S. Department of energy under Contract No. DE-AC05-00OR22725. Funding was provided by the U.S. Department of Energy, Office of Science, Advanced Scientific Computing Research (Field Work Proposals ERKJ381, ERKJ353).

- 
- [1] P. D. Townsend, Simultaneous quantum cryptographic key distribution and conventional data transmission over installed fibre using wavelength-division multiplexing, *Electron. Lett.* **33**, 188 (1997).
- [2] K. A. Patel, J. F. Dynes, I. Choi, A. W. Sharpe, A. R. Dixon, Z. L. Yuan, R. V. Penty, and A. J. Shields, Coexistence of high-bit-rate quantum key distribution and data on optical fiber, *Phys. Rev. X* **2**, 041010 (2012).
- [3] D. Huang, D. Lin, C. Wang, W. Liu, S. Fang, J. Peng, P. Huang, and G. Zeng, Continuous-variable quantum key distribution with 1 Mbps secure key rate, *Opt. Express* **23**, 17511 (2015).
- [4] Y. Mao, B.-X. Wang, C. Zhao, G. Wang, R. Wang, H. Wang, F. Zhou, J. Nie, Q. Chen, Y. Zhao, Q. Zhang, J. Zhang, T.-Y. Chen, and J.-W. Pan, Integrating quantum key distribution with classical communications in backbone fiber network, *Opt. Express* **26**, 6010 (2018).
- [5] I. A. Burenkov, A. Semionov, Hala, T. Gerrits, A. Rahmouni, D. Anand, Y.-S. Li-Baboud, O. Slattery, A. Battou, and S. V. Polyakov, Synchronization and coexistence in quantum networks, *Opt. Express* **31**, 11431 (2023).
- [6] J. M. Thomas, G. S. Kanter, and P. Kumar, Designing noise-robust quantum networks coexisting in the classical fiber infrastructure, *Opt. Express* **31**, 43035 (2023).
- [7] N. A. Peters, P. Toliver, T. E. Chapuran, R. J. Runser, S. R. McNown, C. G. Peterson, D. Rosenberg, N. Dallmann, R. J. Hughes, K. P. McCabe, J. E. Nordholt, and K. T. Tyagi, Dense wavelength multiplexing of 1550 nm QKD with strong classical channels in reconfigurable networking environments, *New J. Phys.* **11**, 045012 (2009).
- [8] P. Eraerds, N. Walenta, M. Legré, N. Gisin, and H. Zbinden, Quantum key distribution and 1 Gbps data encryption over a single fibre, *New J. Phys.* **12**, 063027 (2010).
- [9] I. Choi, R. J. Young, and P. D. Townsend, Quantum key distribution on a 10 Gb/s WDM-PON, *Opt. Express* **18**, 9600 (2010).
- [10] B. Qi, W. Zhu, L. Qian, and H.-K. Lo, Feasibility of quantum key distribution through a dense wavelength division multiplexing network, *New J. Phys.* **12**, 103042 (2010).
- [11] K. A. Patel, J. F. Dynes, M. Lucamarini, I. Choi, A. W. Sharpe, Z. L. Yuan, R. V. Penty, and A. J. Shields, Quantum key distribution for 10 Gb/s dense wavelength division multiplexing networks, *Appl. Phys. Lett.* **104**, 051123 (2014).
- [12] J. C. Chapman, J. M. Lukens, M. Alshowkan, N. Rao, B. T. Kirby, and N. A. Peters, Coexistent quantum channel characterization using spectrally resolved Bayesian quantum process tomography, *Phys. Rev. Appl.* **19**, 044026 (2023).
- [13] J. C. Chapman, A. Miloshevsky, H.-H. Lu, N. Rao, M. Alshowkan, and N. A. Peters, Two-mode squeezing over deployed fiber coexisting with conventional communications, *Opt. Express* **31**, 26254 (2023).
- [14] F. Honz, F. Prawits, O. Alia, H. Sakr, T. Bradley, C. Zhang, R. Slavik, F. Poletti, G. Kanellos, R. Nejabati, P. Walther, D. Simeonidou, H. Hübel, and B. Schrenk, First demonstration of  $25\lambda \times 10$  Gb/s C+L band classical/DV-QKD co-existence over single bidirectional fiber link, *J. Light. Technol.* **41**, 3587 (2023).
- [15] M. Alshowkan, P. G. Evans, B. P. Williams, N. S. V. Rao, C. E. Marvinney, Y.-Y. Pai, B. J. Lawrie, N. A. Peters, and J. M. Lukens, Advanced architectures for high-performance quantum networking, *J. Opt. Commun. Netw.* **14**, 493 (2022).
- [16] W. J. Munro, D. F. V. James, A. G. White, and P. G. Kwiat, Maximizing the entanglement of two mixed qubits, *Phys. Rev. A* **64**, 030302(R) (2001).
- [17] T.-C. Wei, K. Nemoto, P. M. Goldbart, P. G. Kwiat, W. J. Munro, and F. Verstraete, Maximal entanglement versus entropy for mixed quantum states, *Phys. Rev. A* **67**, 022110 (2003).
- [18] N. A. Peters, J. B. Altepeter, D. A. Branning, E. R. Jeffrey, T.-C. Wei, and P. G. Kwiat, Maximally entangled mixed states: Creation and concentration, *Phys. Rev. Lett.* **92**, 133601 (2004).
- [19] C. H. Bennett, H. J. Bernstein, S. Popescu, and B. Schumacher, Concentrating partial entanglement by local operations, *Phys. Rev. A* **53**, 2046 (1996).
- [20] P. G. Kwiat, S. Barraza-Lopez, A. Stefanov, and N. Gisin, Experimental entanglement distillation and ‘hidden’ non-locality, *Nature* **409**, 1014 (2001).

- [21] Z.-W. Wang, X.-F. Zhou, Y.-F. Huang, Y.-S. Zhang, X.-F. Ren, and G.-C. Guo, Experimental entanglement distillation of two-qubit mixed states under local operations, *Phys. Rev. Lett.* **96**, 220505 (2006).
- [22] D. E. Jones, B. T. Kirby, and M. Brodsky, Tuning quantum channels to maximize polarization entanglement for telecom photon pairs, *Npj Quantum Inf.* **4**, 58 (2018).
- [23] B. T. Kirby, D. E. Jones, and M. Brodsky, Effect of polarization dependent loss on the quality of transmitted polarization entanglement, *J. Light. Technol.* **37**, 95 (2019).
- [24] G. Riccardi, C. Antonelli, D. E. Jones, and M. Brodsky, Simultaneous decoherence and mode filtering in quantum channels: Theory and experiment, *Phys. Rev. Appl.* **15**, 014060 (2021).
- [25] N. Gisin, Statistics of polarization dependent losses, *Opt. Commun.* **114**, 399 (1995).
- [26] A. Mecozzi and M. Shtaif, The statistics of polarization-dependent loss in optical communication systems, *IEEE Photon. Technol. Lett.* **14**, 313 (2002).
- [27] C. Eckart and F. R. Shonka, Accidental coincidences in counter circuits, *Phys. Rev.* **53**, 752 (1938).
- [28] B. J. Pearson and D. P. Jackson, A hands-on introduction to single photons and quantum mechanics for undergraduates, *Am. J. Phys.* **78**, 471 (2010).
- [29] M. Alshowkan, J. M. Lukens, H.-H. Lu, B. T. Kirby, B. P. Williams, W. P. Grice, and N. A. Peters, Broadband polarization-entangled source for C+L-band flex-grid quantum networks, *Opt. Lett.* **47**, 6480 (2022).
- [30] H.-H. Lu, M. Alshowkan, K. V. Myilswamy, A. M. Weiner, J. M. Lukens, and N. A. Peters, Generation and characterization of ultrabroadband polarization–frequency hyper-entangled photons, *Opt. Lett.* **48**, 6031 (2023).
- [31] R. Blume-Kohout, Optimal, reliable estimation of quantum states, *New J. Phys.* **12**, 043034 (2010).
- [32] J. M. Lukens, K. J. H. Law, A. Jasra, and P. Lougovski, A practical and efficient approach for Bayesian quantum state estimation, *New J. Phys.* **22**, 063038 (2020).
- [33] H.-H. Lu, K. V. Myilswamy, R. S. Bennink, S. Seshadri, M. S. Alshaykh, J. Liu, T. J. Kippenberg, D. E. Leaird, A. M. Weiner, and J. M. Lukens, Bayesian tomography of high-dimensional on-chip biphoton frequency combs with randomized measurements, *Nat. Commun.* **13**, 4338 (2022).
- [34] M. M. Wilde, *Quantum Information Theory* (Cambridge University Press, Cambridge, United Kingdom, 2017), 2nd ed.
- [35] N. H. Valencia, S. Goel, W. McCutcheon, H. Defienne, and M. Malik, Unscrambling entanglement through a complex medium, *Nat. Phys.* **16**, 1112 (2020).
- [36] H.-H. Lu, J. M. Lukens, B. P. Williams, P. Imany, N. A. Peters, A. M. Weiner, and P. Lougovski, A controlled-NOT gate for frequency-bin qubits, *Npj Quantum Inf.* **5**, 24 (2019).
- [37] H.-H. Lu, N. A. Peters, A. M. Weiner, and J. M. Lukens, Characterization of quantum frequency processors, *IEEE J. Sel. Top. Quantum Electron.* **29**, 6300112 (2023).
- [38] R. T. Thew and W. J. Munro, Entanglement manipulation and concentration, *Phys. Rev. A* **63**, 030302(R) (2001).
- [39] M. Alshowkan, B. P. Williams, P. G. Evans, N. S. V. Rao, E. M. Simmerman, H.-H. Lu, N. B. Lingaraju, A. M. Weiner, C. E. Marvinney, Y.-Y. Pai, B. J. Lawrie, N. A. Peters, and J. M. Lukens, Reconfigurable quantum local area network over deployed fiber, *PRX Quantum* **2**, 040304 (2021).
- [40] P. W. Shor and J. Preskill, Simple proof of security of the BB84 quantum key distribution protocol, *Phys. Rev. Lett.* **85**, 441 (2000).
- [41] M. Koashi and J. Preskill, Secure quantum key distribution with an uncharacterized source, *Phys. Rev. Lett.* **90**, 057902 (2003).
- [42] X. Ma, C.-H. F. Fung, and H.-K. Lo, Quantum key distribution with entangled photon sources, *Phys. Rev. A* **76**, 012307 (2007).
- [43] N. A. Peters, T.-C. Wei, and P. G. Kwiat, Mixed-state sensitivity of several quantum-information benchmarks, *Phys. Rev. A* **70**, 052309 (2004).
- [44] G. Vidal and R. F. Werner, Computable measure of entanglement, *Phys. Rev. A* **65**, 032314 (2002).
- [45] M. B. Plenio, Logarithmic negativity: A full entanglement monotone that is not convex, *Phys. Rev. Lett.* **95**, 090503 (2005).
- [46] I. Devetak and A. Winter, Distillation of secret key and entanglement from quantum states, *Proc. R. Soc. A* **461**, 207 (2005).
- [47] J. Alnas, M. Alshowkan, N. S. V. Rao, N. A. Peters, and J. M. Lukens, Optimal resource allocation for flexible-grid entanglement distribution networks, *Opt. Express* **30**, 24375 (2022).
- [48] G. Vardoyan and S. Wehner, Quantum network utility maximization, [arXiv:2210.08135](https://arxiv.org/abs/2210.08135).